BNL-222068-2021-JAAM

# Glasses denser than the supercooled liquid

Y. Jin, M. Zhernenkov

To be published in "PROCEEDINGS OF THE NATIONAL ACADEMY OF SCIENCES OF THE UNITED STATES OF AMERICA"

August 2021

Photon Sciences

**Brookhaven National Laboratory**

**U.S. Department of Energy**

USDOE Office of Science (SC), Basic Energy Sciences (BES) (SC-22)

# DISCLAIMER

# Glasses Denser than the Supercooled Liquid

**Yi Jin[a], Aixi Zhang[a], Sarah E. Wolf[a], Shivajee Govind[a], Alex R. Moore[b], Mikhail Zhernenkov[c], Guillaume Freychet[c], Ahmad Arabi Shamsabadi[a], and Zahra Fakhraai[a]**

[a]Department of Chemistry, University of Pennsylvania, Philadelphia, PA 19104, USA; [b]Department of Chemical and Biomolecular Engineering, University of Pennsylvania, Philadelphia, PA 19104, USA; [c]NSLS-II, Brookhaven National Laboratory, Upton, NY 11973

This manuscript was compiled on November 13, 2021

**When aged below the glass transition temperature, $T_g$, the density of a glass cannot exceed that of the metastable supercooled liquid (SCL) state, unless crystals are nucleated. The only exception is when another polyamorphic supercooled liquid state exists, with a density higher than that of the ordinary SCL. Experimentally, such polyamorphic states and their corresponding liquid-liquid phase transitions have only been observed in network-forming systems or those with polymorphic crystalline states. In otherwise simple liquids, such phase transitions have not been observed, either in aged or vapor-deposited stable glasses, even near the Kauzmann temperature. Here, we report that the density of thin vapor-deposited films of *N*,*N*'-bis(3-methylphenyl)-*N*,*N*'-diphenylbenzidine (TPD) can exceed their corresponding SCL density by as much as 3.5% and can even exceed the crystal density under certain deposition conditions. We identify a new high-density supercooled liquid (HD-SCL) phase with a liquid-liquid phase transition temperature ($T_{LL}$) ∼35 K below the nominal glass transition temperature of the ordinary SCL. The HD-SCL state is observed in glasses deposited in the thickness range of 25 – 55 nm, where thin films of the ordinary SCL have exceptionally enhanced surface mobility with large mobility gradients. The enhanced mobility enables vapor-deposited thin films to overcome kinetic barriers for relaxation and access the HD-SCL state. The HD-SCL state is only thermodynamically favored in thin films and transforms rapidly to the ordinary SCL when the vapor deposition is continued to form films with thicknesses more than 60 nm.**

Physical vapor deposition | Thin film mobility | Stable glass | Mobile surface layer | Liquid-liquid phase transition

Glasses are formed when the structural relaxations in supercooled liquids (SCL) become too slow, causing the system to fall out of equilibrium at the glass transition temperature ($T_g$). The resulting out-of-equilibrium glass state has a thermodynamic driving force to evolve towards the supercooled liquid state through physical aging (1). At temperatures just below $T_g$, the extent of equilibration is limited by the corresponding SCL state, while at much lower temperatures, equilibration is limited by the kinetic barriers for relaxation. As such, the degree of thermodynamic stability achieved through physical aging is limited (2).

Physical vapor deposition (PVD) is an effective technique to overcome kinetic barriers for relaxation to produce thermodynamically stable glasses (SGs) (3–10). The accelerated equilibration in these systems is due to their enhanced surface mobility (11–14). During physical vapor deposition, when the substrate temperature is held below $T_g$, molecules or atoms can undergo rearrangements and adopt more stable configurations at the free surface and proximate layers underneath (13). Once the molecules are buried deeper into the film their relaxation dynamics significantly slow down, which prevents further equilibration. Through this surface-mediated equilibration process stable glasses can achieve low-energy states on the potential energy landscape that would otherwise require thousands or millions of years of physical aging (2, 3, 15, 16).

As such, the degree of enhanced surface mobility and mobility gradients are critical factors in the formation of stable glasses (3, 11, 17, 18). While the effect of film thickness on the surface mobility and gradients of liquid-quenched glasses has been studied in the past (19, 20), there is limited data on the role of film thickness in the stability of vapor-deposited glasses. In vapor-deposited toluene, it has been shown that decreasing the film thickness from 70 nm to 5 nm can increase the thermodynamic stability but decrease the kinetic stability (5, 6). In contrast, thin films covered with a top layer of another material do not show a significant evidence of reduced kinetic stability (21), indicating the non-trivial role of mobility gradients in thermal and kinetic stability.

Stable glasses of most organic molecules, with short-range intramolecular interactions, have properties that are indicative of the same corresponding metastable SCL state as liquid-quenched (LQ) and aged glasses, without any evidence of the existence of generic liquid-liquid phase transitions that can potentially provide a resolution for the Kauzmann entropy crisis (22). The Kauzmann crisis occurs at the Kauzmann temperature ($T_K$), where the extrapolated SCL has the same structural entropy as the crystal, producing thermodynamically impossible states just below this temperature. Recently,

## Significance Statement

Enhanced surface mobility enables rapid equilibration of vapor-deposited glasses towards the supercooled liquid (SCL). We demonstrate that thin films of TPD molecular glass, when vapor-deposited below a certain temperature, can access a high-density SCL (HD-SCL) state through a liquid-liquid phase transition ∼35 K below the nominal glass transition temperature of ordinary SCL. The HD-SCL phase transforms into the ordinary SCL when the thickness is increased above 60 nm, demonstrating that HD-SCL is only thermodynamically favored in thin films. These results provide a recipe for accessing otherwise kinetically inaccessible regions in the energy landscape, which are critical for understanding the glass transition phenomenon. Access to high-density stable glass states that can resist crystallization and dewetting are also important in various applications.

Y.J. performed the majority of the sample preparation and characterization experiments. A.Z, S.G., and S.E.W. contributed to the construction and maintenance of the ultra-high vacuum chamber for PVD experiments. A.Z., S.G, A.R.M., M.Z., and G.F. performed the GIWAXS experiments. A.A.S. performed the powder XRD and UV-vis absorption experiments. Y.J., A.Z., S.G., S.E.W., A.R.M., and Z.F. analyzed the data. Y.J. and Z.F. wrote the manuscript, with input from all other researchers. Z.F. directed the research.

The authors declare no competing interests.

[2]To whom correspondence should be addressed. E-mail: fakhraai@sas.upenn.edu

Ediger *et al.* showed that near-equilibrium states of ethylbenzene can be produced using PVD down to 2 K above $T_K$, and hypothesized that any phase transition to an "ideal glass" state to avoid the Kauzmann crisis must occur at $T_K$ (16).

In some glasses of elemental substances (23, 24) and hydrogen-bonding compounds (25, 26), liquid-liquid phase transitions can occur between polyamorphic states with distinct local packing structures that correspond to polymorphic crystalline phases. For example, at high pressures, high- and low-density supercooled water phases are inter-convertible through a first-order phase transition (27, 28). Recent studies have demonstrated that such polyamorphic states can also be accessed through physical vapor deposition in hydrogen bonding systems with polymorphic crystal states at depositions above the nominal $T_g$ (29, 30). However, these structure-specific transitions do not provide a general resolution for the Kauzmann crisis.

Here, we report the observation of a liquid-liquid phase transition in vapor-deposited thin films of *N*,*N*'-bis(3-methylphenyl)-*N*,*N*'-diphenylbenzidine (TPD). TPD is a molecular glassformer with only short-range intermolecular interactions. When thin films of TPD are vapor deposited onto substrates held at deposition temperatures ($T_{dep}$) below the nominal glass transition temperature of bulk TPD, $T_g$(bulk), films in the thickness range of 25 nm $< h <$ 55 nm achieve a new high-density supercooled liquid (HD-SCL) state. The liquid-liquid phase transition temperature ($T_{LL}$) between the ordinary SCL and HD-SCL states is measured to be $T_{LL} \simeq T_g$(bulk) $-$ 35 K. The density of thin films deposited below $T_{LL}$ tangentially follow the HD-SCL line, which has a stronger temperature dependence than the ordinary SCL. When vapor deposition is continued to produce thicker films ($h >$ 60 nm), the HD-SCL state transforms into the ordinary SCL state, indicating that the HD-SCL is only thermodynamically favored in the thin film geometry. This transition is qualitatively different than the previously reported liquid-liquid phase transitions, as it is not related to a specific structural motif in TPD crystals and it can only be observed in thin films, indicating that the energy landscape of thin films is favoring this high-density state.

We observe an apparent correlation between enhanced mobility gradients in liquid-quenched thin films of TPD and the thickness range where HD-SCL states are produced during PVD. We hypothesize that enhanced mobility gradients are essential in providing access to regions of the energy landscape corresponding to the HD-SCL state which are otherwise kinetically inaccessible. This hypothesis should be further investigated to better understand the origin of this phenomenon.

## Results

**Structural Characterization of Vapor-Deposited Films.** Physical vapor deposition was used to produce smooth and uniform TPD thin films as detailed in the Materials and Methods section and the online Supplementary Information (SI). Figure 1 shows the in-plane ($q_{xy}$) and out-of-plane ($q_z$) grazing incidence wide angle X-ray scattering (GIWAXS) data for films deposited at a substrate deposition temperature of $T_{dep} = 264 \pm 3$ K, as well as a 200 nm liquid-quenched glass film. The two-dimensional data used to extract these spectra are shown in Figure S10. X-ray diffraction measurements of TPD crystal is shown in Figure S11 as a reference. The GIWAXS

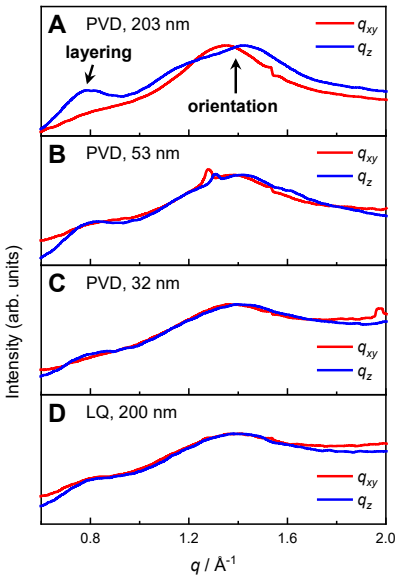


**Fig. 1.** In-plane ($q_{xy}$) and out-of-plane ($q_z$) GIWAXS scattering intensity for films vapor deposited at $T_{dep} = 264 \pm 3$ K with thicknesses of (A) 203 nm, (B) 53 nm, and (C) 32 nm, and (D) a 200 nm liquid-quenched (LQ) glass film. The anisotropic features observed in (A) can be attributed to molecular orientation ($q \sim 1.4$ Å$^{-1}$) and layering ($q \sim 0.8$ Å$^{-1}$), respectively.

data for the 203 nm vapor-deposited film (Figure 1A) shows a noticeable difference between the scattering intensity along the in-plane $q_{xy}$ and out-of-plane $q_z$ directions, indicating a significant anisotropy in this film. In contrast, the 200 nm liquid-quenched film (Figure 1D) has a broad isotropic scattering signal, which is typically observed in liquid-quenched glasses. The anisotropy of the thick PVD film is consistent with previous observations in TPD (31, 32) and other stable glass systems (31–36). In the data shown in Figure 1A, the anisotropy observed in the intra-molecular scattering region ($q \sim$1.4 Å$^{-1}$, $\sim$0.5 nm length-scale) is attributed to orientational order of TPD molecules (31), while the peak observed in the out-of-plane direction at $q_z \sim 0.8$ Å$^{-1}$ ($\sim$ 0.8 nm length scale) is due to molecular layering normal to the film surface (35, 37). This feature has been observed in a broad range of stable glasses (31, 37, 38). As the film thickness is reduced at this deposition temperature, the differences between $q_{xy}$ and $q_z$ are diminished (Figures 1B & C) and the films become more isotropic, but films of all thicknesses remain amorphous, with no sign of crystallization.

Spectroscopic ellipsometry was also used to evaluate the structural anisotropy of as-deposited films, through measurements of optical birefringence (35, 39) (more details in Materials and Methods section and SI). In thick TPD films ($h >$ 60 nm), birefringence strongly varies with the deposition temperature, becoming more negative at lower $T_{dep}$, indicating preferred in-plane molecular orientation, consistent with the GIWAXS data (Figures 1 and S10) and previous studies (31, 36). In contrast, films with $h <$ 60 nm show zero or small positive birefringence values when the ellipsometry data is fit to a birefringent optical model. However, the error in defining birefringence in ellipsometry measurements increases with decreasing film thickness (detailed in SI and Figure S15). As such, given the reduced anisotropy observed in GIWAXS experiments (Figure 1), isotropic fitting was used to fit the

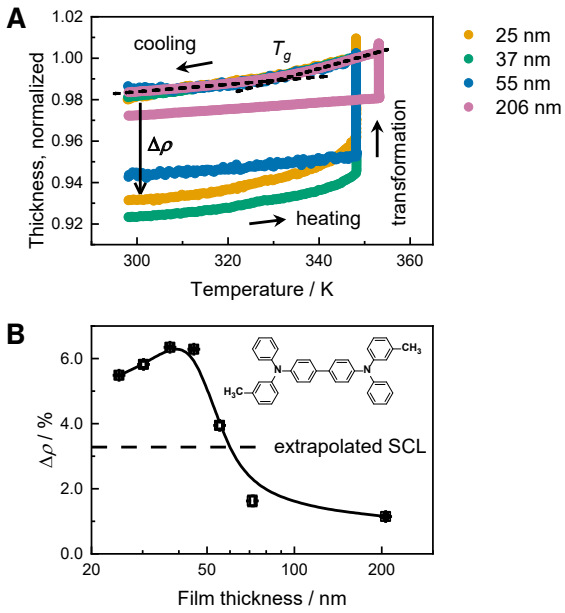


**Fig. 2.** (A) Normalized thickness vs. temperature during dilatometry cycles for films deposited at $T_{\rm dep} = 264 \pm 3$ K. Dashed black lines are linear fits to the SCL and liquid-quenched glass regions of the 206 nm film to determine $T_g({\rm bulk}) = 330 \pm 2$ K. The long black arrow shows the determination of relative density ($\Delta\rho$) for the 25 nm film with respect to its liquid-quenched glass state. Short arrows show the direction of the thermal cycle. (B) $\Delta\rho$ (evaluated at 298 K) vs. film thickness. The horizontal dashed line shows $\Delta\rho$ of the extrapolated ordinary SCL at 264 K ($\Delta\rho_{\rm SCL} = 3.3 \pm 0.2\%$). The inset shows the molecular structure of TPD. Some error bars in (B) are smaller than the symbol size.

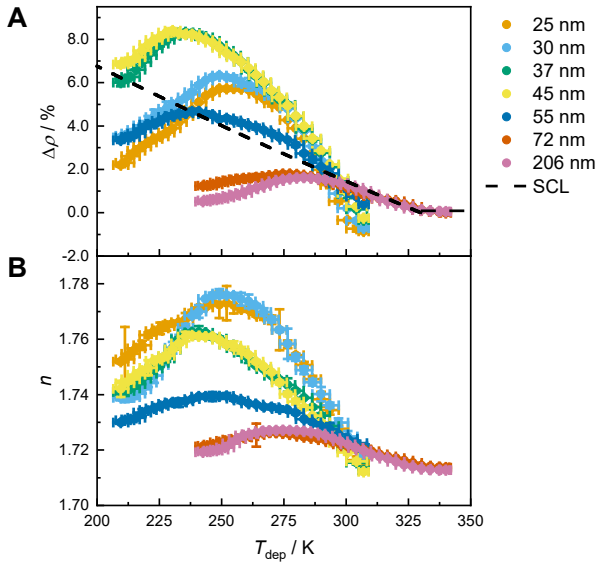


**Fig. 3.** (A) Relative density change, $\Delta\rho$, vs. deposition temperature, $T_{\rm dep}$, for $T$-grad films with various thicknesses. The dashed line shows the extrapolated density of bulk SCL. (B) Index of refraction ($n$) of as-deposited films vs. $T_{\rm dep}$, measured at the wavelength $\lambda = 632.8$ nm. For the 72 nm and 206 nm films, which are birefringent, the average value of $n$ is plotted.

data for films with $h < 60$ nm. We note that the choice of the model (birefringent vs. isotropic) does not affect the measured film thicknesses and the calculated density (Figure S16B).

**Dilatometry Experiments.** Figure 2A shows ellipsometry-based dilatometry measurements for films vapor-deposited at $T_{\rm dep} = 264 \pm 3$ K. Films of all thicknesses have higher initial density (lower initial film thickness) compared to their transformed liquid-quenched states as shown in Figure 2B. As the film thickness is decreased, the relative density ($\Delta\rho$) is increased dramatically, reaching a maximum at $h \sim 40$ nm. $\Delta\rho$ decreases slowly as the film thickness is further decreased. It is notable that for $h < 60$ nm, $\Delta\rho$ exceeds the extrapolated density of the supercooled liquid at $T_{\rm dep} = 264 \pm 3$ K (dashed line in Figure 2B). The initial film density can also be independently evaluated through measurements of the index of refraction, $n$, which is related to the density through the Lorentz-Lorenz relationship (40). Figure S19 shows that films of all thicknesses also have higher initial average index of refraction compared to their transformed states, in agreement with the dilatometry results in Figure 2A.

To further investigate the effect of deposition temperature and film thickness on the relative density change ($\Delta\rho$) and index of refraction ($n$), TPD films were vapor deposited on substrates with a temperature gradient ($T$-grad) along their long axis (details in Materials and Methods as well as in SI). This high-throughput method allows simultaneous depositions at a broad range of $T_{\rm dep}$ values (33, 41). Figure 3 shows $\Delta\rho$ and $n$ vs. $T_{\rm dep}$ for $T$-grad films of various thicknesses. For films with $h > 50$ nm, where a birefringent model was used to fit the ellipsometry data, the average index of refraction is shown in Figure 3B. The corresponding birefringence data is shown in Figure **??** (details of measurements and calculations in SI). Figure 3A shows that in thick films ($h > 60$ nm), $\Delta\rho$ is limited by the extrapolated density of the supercooled liquid ($\Delta\rho\,({\rm SCL})$, dashed line) and does not exceed this value. Close to the nominal $T_g({\rm bulk})$, the density of as-deposited films can reach this limiting value, while at lower $T_{\rm dep}$ values, the system is kinetically trapped with $\Delta\rho < \Delta\rho\,({\rm SCL})$. This observation is similar to the previous reports in stable glasses of TPD and other molecules (7, 16, 33, 39).

In thin films ($h < 60$ nm), remarkably high values of density are observed (Figure 3A) and $\Delta\rho$ well exceeds the extrapolated SCL density. For example, at $T_{\rm dep} = 264$ K, $\Delta\rho\,({\rm SCL}) = 3.3 \pm 0.2\%$, while for 45 nm vapor-deposited film, $\Delta\rho = 6.3\%$. These trends continue as $T_{\rm dep}$ is further decreased, with a maximum $\Delta\rho$ of 8.4% achieved in 37 nm and 45 nm films deposited at $T_{\rm dep} \sim 230$ K. High density states are also seen in 30 nm and 25 nm films, but to a smaller extent. The index of refraction ($n$) of as-deposited films also increases dramatically as the film thickness is decreased (Figure 3B), providing additional independent evidence for the dramatic density increase in vapor-deposited thin films. Using $n$, the estimated density of the 30 nm and 25 nm films appear to exceed those of 45 nm and 55 nm films for 240 K $< T_{\rm dep} <$ 300 K. This difference in the observed trends can be explained by the fact that $\Delta\rho$ is calculated relative to the transformed liquid-quenched state, while $n$ is directly measured in as-deposited films. We observe that the indices of refraction of the supercooled liquid and liquid-quenched glass states are also increased in thin films compared to their bulk values (Figure S22), resulting in smaller relative $\Delta\rho$ when values are compared. If relative $\Delta n$ values were used instead of $n$, trends would be very similar to those observed with $\Delta\rho$, as $\Delta n$ is strongly correlated with $\Delta\rho$ (Figure S21, more details in SI).

The observation that the index of refraction of the supercooled liquid is increased in thin films (Figure S22) indicates that the density of the SCL state is also higher in thin films than that of the bulk. A similar effect was previously observed in polymer thin films (42, 43), but its origins are not well understood and should be further investigated. However, we also note that the error in evaluating $n$ also increases with decreasing film thickness. As such, we opt to frame the discussions in this manuscript around $\Delta\rho$ obtained based on film thickness, providing a more conservative estimation of the magnitude of the observed phenomenon.

Another factor that affects the calculated $\Delta\rho$ is the fact that the glass transition temperature of thin TPD films are lower than $T_g$(bulk) (19). As such, each sample is compared to a slightly different reference state. To eliminate this effect, we present the data using the estimated specific volume ($V_{\rm sp}$) of each film at the deposition temperature, $T_{\rm dep}$ (Figure 4).

## Discussions

**Polyamorphism in Thin Films.** Figure 4A shows a plot of normalized specific volume ($V_{\rm sp}$) vs. $T_{\rm dep}$ for films of various thicknesses (detailed calculations in SI). The $V_{\rm sp}$ values for all samples were normalized to their corresponding supercooled liquid state at 348 K. As seen in Figure 4A, in thick films ($h > 60$ nm) deposited at $T_{\rm dep} > 310$ K, the as-deposited glass reaches the same specific volume as the corresponding SCL state, implying that these films have enough surface mobility during vapor deposition to reach the metastable equilibrium state and do not further evolve. At $T_{\rm dep} < 300$ K, thick films do not have enough mobility and their $V_{\rm sp}$ increases towards that of the liquid-quenched glass state. This data is consistent with previous studies that identify the SCL state as the limiting state achieved during physical vapor deposition (33, 37, 39).

The temperature dependence of $V_{\rm sp}$ is remarkably different in films with $h < 60$ nm. In these films, the limiting value of $V_{\rm sp}$ appears along a line with a higher slope than that of the extrapolated bulk SCL line. This apparent new high-density supercooled liquid state (HD-SCL) was previously unidentified in TPD. The trends of $V_{\rm sp}$ vs. $T_{\rm dep}$ with respect to this new limiting HD-SCL state are qualitatively similar to what is observed in thick films with respect to the ordinary SCL state; as $T_{\rm dep}$ is decreased, $V_{\rm sp}$ reaches a minimum at some low deposition temperature, where the system is no longer able to kinetically reach this metastable HD-SCL state, and deposition below this point produces glasses with higher specific volume and lower density than the extrapolated HD-SCL line.

The liquid-liquid phase transition between the two polyamorphic SCL and HD-SCL states is observed at $T_{LL} \simeq 295 \pm 5$ K ($\sim 35$ K below the nominal $T_g$(bulk) of the SCL) and is relatively abrupt. As shown in Figure 4B, when $T_{\rm dep}$ is well above $T_{LL}$ (i.e. $T_{\rm dep} > 320$ K), $V_{\rm sp}$ reaches the $V_{\rm sp}$ of the ordinary SCL and does not further evolve, indicating that the ordinary SCL is the energetically favored state in this deposition range. As $T_{\rm dep}$ is decreased, after a transition region with non-monotonic density change ($295$ K $< T_{\rm dep} < 320$ K), the $V_{\rm sp}$ of vapor-deposited thin films follow the HD-SCL line. For $270$ K $< T_{\rm dep} < T_{LL}$, the surface mobility appears to be high enough for these films to reach the new corresponding equilibrium, which is the HD-SCL state. The specific volume reaches a minimum value around $T_{\rm dep} \sim 230$ K ($0.78\,T_{LL}$) in 37 – 45 nm films, below which the samples appear to be kinetically trapped, relative to the extrapolated HD-SCL.

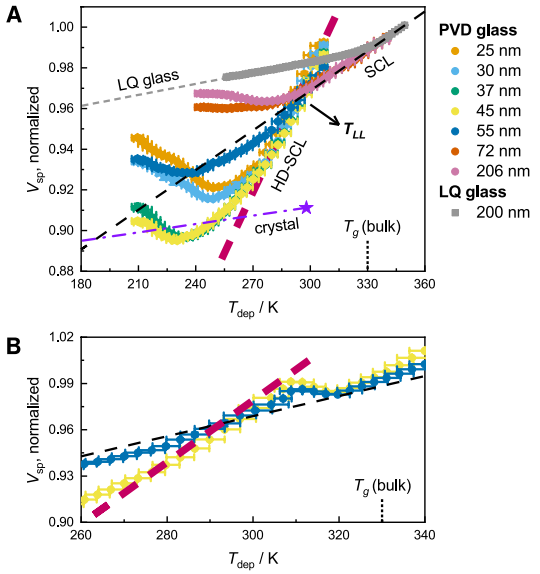


**Fig. 4.** (A) Normalized specific volume ($V_{\rm sp}$) vs. $T_{\rm dep}$ for $T$-grad films of various thicknesses. The cooling curve of a 200 nm liquid-quenched (LQ) glass is shown as reference (10 K/min cooling, extrapolated by the gray dotted line). The black dashed line is the extrapolated supercooled (SCL) liquid line for this film. The thick red dashed line shows the apparent marginal specific volume for thin films, assigned as the high-density SCL (HD-SCL) state. $T_{LL}$ (small black arrow) indicates the location of phase transition between SCL and HD-SCL states. The purple dashed-dotted line shows the estimated $V_{\rm sp}$ of the monoclinic TPD crystal vs. temperature, based on the crystal density measured at 298 K (star symbol, Ref. 44) and 90 K (Ref. 45, point not shown). (B) Normalized $V_{\rm sp}$ vs. $T_{\rm dep}$ for 45 nm and 55 nm $T$-grad films for an extended $T_{\rm dep}$ range. In both graphs, $T_g$(bulk) for liquid-quenched TPD is indicated for reference.

As shown in Figure 1, despite their exceptionally high density, thin films produced in the HD-SCL state are amorphous and do not show any sign of crystallization. Without the existence of a liquid-liquid phase transition, it is impossible to produce amorphous states with densities larger than SCL. The evidence for a phase transition is strengthened when we focus on the films deposited in the region close to $T_{LL}$ (Figure 4B). We observe a transition region in the deposition range of $T_{LL} < T_{\rm dep} < 320$ K, where the specific volume in thin films changes non-monotonically. The specific volume follows the $V_{\rm sp}$ of the ordinary SCL above this deposition range and the $V_{\rm sp}$ of the HD-SCL below this range. The non-monotonic change in $V_{\rm sp}$ can be a sign of phase transition, where in this region a co-existing mixture of the two phases are deposited resulting in this non-trivial behavior. In this region, we also observe high surface roughness in as-deposited thin films (AFM images shown in Figures S7 – S9). The increased roughness may be interpreted as a sign of enhanced surface mobility and mobility gradients in vapor-deposited films, similar to what has been previously observed in liquid-quenched TPD films (19). However, enhanced mobility is expected to make more stable glasses with lower $V_{\rm sp}$ values, which is not the case here. Alternatively, the roughness can be an indirect sign of proximity to a phase transition, which can cause large volume fluctuations and thus larger surface roughness. Regardless, above and below this transition region the specific volume clearly follows two distinct slopes, which intersect at $T_{LL}$, providing a strong evidence for polyamorphism in thin films.

It is therefore also possible that the actual phase transition point is in the region with maximum density (the middle of the co-existence region). More detailed experiments in this transition region, as well as direct calorimetry experiments should be employed in the future to provide further insight into details of this liquid-liquid transition.

Without polyamorphism the values of enthalpy and specific volume cannot decrease below their corresponding SCL values either through physical aging or vapor deposition (7, 34, 39). Beasley *et al.* recently showed that in $\sim$ 400 nm films of ethylbenzene the density of vapor-deposited glasses follow the extrapolated SCL density down to 2 K above the Kauzmann temperature (16). As such, it has been hypothesized that any resolution of the Kauzmann crisis will occur at $T_{\mathrm{K}}$ for bulk systems. Our data shown in Figure 4A paints a remarkably different picture in thin films, where geometrical constraints appear to produce a modified energy landscape where an amorphous packing with exceptionally high density can be equilibrated during vapor deposition. In thin films molecules are packed in significantly closer proximity than both known crystal forms of TPD, the monoclinic and the orthorhombic crystals (44, 45) (values listed in SI). In thick films, the crystal state is the equilibrium phase that minimizes the free energy. In thin films deposited below $T_{LL}$, the HD-SCL is expected to have a lower free energy than the SCL state. While this phase has a higher density than the bulk crystal, it is not immediately clear whether a corresponding crystal state also exist in thin films with higher density than the bulk crystal. However, we have not observed any evidence of crystallization in our experiments, which indicates that the HD-SCL may indeed be the equilibrium phase that minimizes the free energy as opposed to a metastable phase. Regardless, the observation of the phase transition is a strong evidence that the thin film geometry can equilibrate amorphous structures that are not otherwise thermodynamically favored in bulk films.

It is important to note that our data does not necessarily offer a resolution for the Kauzmann crisis. Given the large slope of the HD-SCL compared to the ordinary SCL, the apparent Kauzmann temperature is even higher for the HD-SCL state and is estimated to be at $T_{\mathrm{K}}(\text{HD-SCL}) \simeq 265$ K as opposed to $T_{\mathrm{K}}(\text{SCL}) \simeq 190$ K for bulk films (Figure S18 shows corresponding fictive temperatures of vapor-deposited films with respect to each state). Furthermore, in the temperature range of 220 K $< T_{\mathrm{dep}} <$ 250 K the density actually exceeds that of the crystal. However, density is not the correct metric for the Kauzmann crisis and one needs to evaluate the corresponding entropy of each state with respect to the crystal entropy. While in the ordinary SCL the density typically follows the trends in entropy, there is no thermodynamical reason why this should also be the case for HD-SCL. To our knowledge these are some of the highest density states ever seen in molecular glasses in ambient pressures. As such, understanding the details of this packing, its corresponding structural entropy, and how the thin film geometry enables its equilibration merit further studies.

**The Role of Surface Mobility in Accessing HD-SCL.** A major contrast between the polyamorphism observed here and those previously seen in bulk stable glasses is that the $T_{LL}$ in TPD thin films is well below its nominal $T_g$(bulk). In bulk TPD, the estimated relaxation time at 295 K (where $T_{LL}$ is measured here) is $\sim 10^{22}$ sec ($\sim 10^{14}$ years) (12). As such, even if the HD-SCL could exist in the bulk, it would not be accessible through physical aging. Even during vapor deposition, at $T_{\mathrm{dep}} = 295$ K thick films are in kinetically trapped states, making the HD-SCL inaccessible for these films.

During physical vapor deposition, stable glasses are formed because of the enhanced mobility at the free surface (3, 11, 36, 46) and layers directly underneath (13, 17). Surface mobility gradients allow molecules in the surface region to adopt more efficient packing structures, before falling out of equilibrium at locations deeper into the film. The ability to access the otherwise inaccessible HD-SCL by thin films is a strong evidence that the dynamics near the surface region of thin films are significantly enhanced compared to those of thick films. This relatively enhanced mobility would allow thin films to equilibrate into the HD-SCL state at low deposition temperatures. There is indirect evidence for this hypothesis in measurements of liquid-quenched TPD films. Measurements of mobility in thin liquid-quenched TPD films (19) as well as measurements of the breadth of the $T_g$ transition (20) show that they have faster mobility at the free surface and enhanced mobility across their entire thickness. When comparing $\Delta\rho$ in vapor-deposited films with the breadth of the $T_g$ transition in liquid-quenched counterparts (Figure S25), it appears that the highest density films produced during PVD are in the thickness range where liquid-quenched films still have some portions with slow, bulk-like mobility (presumably in regions close to the substrate), producing a broad mobility gradients in these films. In thinner films ($h < 35$ nm), mobility of liquid-quenched films are enhanced throughout their thickness, and PVD films show a smaller extent of density increase (more details in SI). We interpret these observations to mean that in order to produce a stable glass, sufficient enhanced mobility needs to be coupled with the ability to fall out of equilibrium deep inside the film. The details of this correlation and the specific pathways towards different regions in the energy landscape merit further future studies.

Another strong indication for the role of enhanced mobility gradients in accessing the HD-SCL state, is the observation that thin PVD films are more isotropic that thick films, based on both the limited GIWAXS data for films deposited at $T_{\mathrm{dep}} = 264$ K (Figure 1) and the birefringence values when the ellipsometry data in thin films is fit to a birefringent model (Figure S16). It has been previously demonstrated that slower deposition rates can produce more isotropic stable glasses (47), because the molecules have a chance to equilibrate at layers well below the free surface. As such, the templated orientation at the free surface region can be erased. Recent computer simulations have also provided evidence for reorientation below the free surface (13) during vapor deposition. In TPD thin films, the longer range of mobility gradients compared to the bulk films can have a similar effect in reducing their orientational anisotropy, analogous to a change in the deposition rate.

While it is not clear whether the HD-SCL state is ubiquitous in vapor deposited thin films, enhanced surface and thin film mobility has been broadly observed in organic and polymeric thin films (5, 48–51). As such, it is likely that the strong variations in mobility gradients due to the free surface and its interplay with substrate interactions would significantly affect stable glass formation in films with intermediate thicknesses. For example, one can hypothesize that using a substrate with

more favorable interactions, which affects the mobility gradients (20), would also produce highly stable glasses or HD-SCL states in even thinner films. This can provide an exciting opportunity to produce ultra-thin stable glass films with varying degrees of orientational order and stability, through an interplay between the surface and substrate dynamics. While their liquid-quenched counterparts can rapidly dewet or crystallize (19, 51), hindering their applications, vapor-deposited films can be produced with lower roughness and better thermal stability, with exceptionally high density.

**The Importance of Thin Film Geometry in the Stabilization of HD-SCL.** A unique and unexpected feature of the data presented in this study, is the rapid transformation of thin film from HD-SCL state to a much lower density state upon continued deposition. For example, as seen in Figure 3A, at $T_{\rm dep} = 230$ K, 37 nm and 45 nm films have nearly the same density ($\Delta\rho = 8.4\%$). However, upon the deposition of another 10 nm, the 55 nm film has an average density of $\Delta\rho = 4.5\%$. Increasing the film thickness further to 206 nm results in a film that is marginally stable, with a density even lower than that of the ordinary SCL. If the bottom 45 nm of the film remained at the same initial HD-SCL density while the deposition continued, one would expect the 206 nm film to have at least a density of $\Delta\rho = 1.8\%$, which is not the case. This means that as the deposition is continued, the entire film actually dilates and transforms into a different corresponding state, presumably to that of the ordinary SCL. Future *in situ* measurements and computer simulations are needed to elucidate the details of this phenomenon.

It is difficult to rationalize this phenomenon without assuming that thin films have distinctly different equilibrium states than thick films. This is a strong evidence that the geometry and boundary conditions in thin films produce a unique energy landscape, which allows an otherwise thermodynamically disfavored phase (HD-SCL) to become the equilibrium phase in thin films. This is analogous of a tilting of the energy landscape due to an external driving force. Once the thickness exceeds the point where the Gibbs free energy of this state is higher than that of the ordinary SCL, the system returns to the ordinary SCL, resulting in the rapid observed transformation. This hypothesis can explain the non-trivial behavior of the 55 nm film with respect to $T_{\rm dep}$, which appears to fall somewhere between the SCL and HD-SCL lines depending on the deposition temperature (Figure 4A). This hypothesis would also imply that the 55 nm films still has enough enhanced mobility, even at $T_{\rm dep} = 230$ K to entirely transform from HD-SCL to SCL upon PVD. Interestingly, by the time a 200 nm film is deposited, the film mobility even at its free surface is so low that it cannot even form a typical stable glass. This collective behavior suggests that surface mobility and mobility gradients strongly depend on both the film thickness and temperature, which is also supported by limited existing data in liquid-quenched thin films (19, 20, 50).

However, it is still surprising that the 55 nm continues to evolve into a less-dense state, to produce a marginally stable state when the thickness reaches 200 nm. Based on measurements of mobility in liquid-quenched TPD films (19, 20), we do not expect these films to have equilibrium relaxation times that are fast enough to evolve into the ordinary SCL state. Indeed if that was the case, we would expect the system to stop evolving once ordinary SCL state was achieved, which is significantly higher density than is observed in 200 nm films at low deposition temperatures. The only possible justification is that once the energy landscape is tilted to make the ordinary SCL the equilibrium state for the thick films, a driving force is generated for the system to rapidly dilate. This phenomenon appears analogous to volume recovery of pressurized glasses after the pressure is removed (52) or memory effects in physical aging after a temperature up-jump event (53, 54), both of which result in volume evolution that is faster than the nominal relaxation times in these systems. Here, the change in the energy landscape from the thin film geometry to the bulk state appears to trigger a similar effect, resulting in an apparent dilation that is faster than the equilibrium relaxation times of the system. However, this connection is not immediately trivial or clear. *In situ* experiments to measure volume recovery upon rapid vapor deposition or flash DSC experiments to measure whether strong changes in activation entropy occur due to the changing boundary conditions can be employed to further study this rather surprising phenomenon (55).

The origins of widely changing dynamical gradients and their corresponding thickness effects in thin films themselves remain poorly understood (20). The data here indicates that depending on the method of preparation (quenching the liquid versus physical vapor deposition) either liquid-like (dewetting, low $T_g$) or stable and dense states (corresponding to HD-SCL), can be achieved that belong to distinctly different regions in the energy landscape. However, regardless of their nature, most of these effects, including the observation of higher density values in liquid-quenched and ordinary SCL films (Figure S22) rapidly disappear when the film thickness is increased above 60 nm. As such, thin films can be strong candidates to experimentally explore various theories of glass transition and their validity in deeply supercooled states as well as at small length scales. The existence of similar effects in other glassy systems should be explored to evaluate the generality of this phenomenon.

## Conclusions

We have demonstrated that vapor-deposited thin films of molecular glass TPD produce amorphous states with densities much higher than the ordinary supercooled liquid state. Screening across a wide range of deposition temperatures, we identify a high-density SCL state (HD-SCL) with a liquid-liquid transition temperature $T_{LL} \approx T_g(\text{bulk}) - 35$ K. The densest glasses have densities that are comparable or higher than the TPD crystal. The HD-SCL state is produced at a thickness range where large mobility gradients are also observed in liquid-quenched TPD films (37 nm $< h <$ 45 nm), providing a strong correlation between enhanced mobility gradients and ability to kinetically access the polyamorphic HD-SCL state. Upon further deposition, films with thicknesses of 50 nm and higher rapidly dilate and lose their high-density conformations, demonstrating that the HD-SCL state is only thermodynamically favored in the thin film geometry, enabled by its unique energy landscape.

## Materials and Methods

TPD (structure shown in Figure S1) was used as purchased (MilliporeSigma). The bulk glass transition temperature was determined by differential scanning calorimetry (DSC, TA Instruments, Q2000) to be $T_g(\text{bulk}) = 330 \pm 2$ K (Figure S2). TPD powder was premelted in a vacuum oven (Fisherbrand Isotemp Model 281A) before

use. TPD was thermally evaporated on silicon substrates (Virginia Semiconductor), bridged between two independently temperature-controlled (Omega controllers) stages in a custom ultra-high vacuum chamber (base pressure $\sim 2 \times 10^{-7}$ Torr) (17, 56). A temperature gradient ($T$-grad) was established across the two stages for high-throughput sample preparation. More details of sample preparation and temperature control can be found in SI and Figures S3 – S5. The variation of film thickness along the $T$-grad samples was below 3% of the average film thickness (Figure S6). All depositions were performed at a deposition rate of $r_{\rm dep} = 0.030 \pm 0.005$ nm/s.

Atomic force microscopy (AFM, Agilent 5420) was used to characterize surface morphology. Except for the data shown in Figure 4B, the data reported here were limited to samples with as-deposited root mean square (RMS) roughness less than 2 nm, to reduce uncertainties of thickness measurements (details in SI, and Figures S7 and S8). AFM was also performed on samples after dilatometry to rule out dewetting or crystallization (Figure S9).

Grazing incidence wide angle X-ray scattering (GIWAXS) measurements were conducted at the National Synchrotron Light Source II, Brookhaven National Laboratory, with a beam energy of 18.2 keV (details in SI).

Variable-angle spectroscopic ellipsometry (J. A. Woollam M-2000) was performed to determine the thickness ($h$), indices of refraction $n_{xy}$ and $n_z$, and optical birefringence, $\delta n = n_z - n_{xy}$ of as-deposited films (details in Figures S14 – S16). Dilatometry experiments were performed by heating as-deposited films at 10 K/min, to either 348 K and holding for 20 min for thin films, or to 353 K and holding for 30 min for thick films, to complete the transformation. The films were subsequently cooled at 10 K/min to 298 K to form liquid-quenched glasses. The film thickness and indices of refraction were measured *in situ* during dilatometry, at a frequency of 2.5 s with zone averaging, at an angle of incidence of 70° (Figures 2A and S19). Using this data, the fictive temperature ($T_f$), liquid-quenched $T_g$, and the onset of transformation ($T_{\rm onset}$) values were determined (Figures S17 and S18). $\Delta\rho$ was evaluated based on the initial and final thickness of the films, measured at 298 K, at an array of locations across the $T$-grad sample using variable-angle spectroscopic ellipsometry, from where their specific volumes ($V_{\rm sp}$) were deduced (more details in SI).

**ACKNOWLEDGMENTS.** The authors would like to thank Robert A. Riggleman, Richard B. Stephens, Mark D. Ediger, Connie B. Roth, and Russell J. Composto for helpful discussions. This research used the Soft Matter Interfaces (SMI, Beamline 12-ID) of the National Synchrotron Light Source II, a U.S. Department of Energy (DOE) Office of Science User Facility operated for the DOE Office of Science by Brookhaven National Laboratory under Contract No. DE-SC0012704. This work was funded by an NSF-DMR (DMREF-1628407) grant and the University of Pennsylvania Materials Research Science and Engineering Center, MRSEC (NSF-DMR-1720530). The authors acknowledge the use of facilities at the Laboratory for Research on the Structure of Matter at the University of Pennsylvania. A.A.S. was supported by a postdoctoral fellowship from the Vagelos Institute for Energy Science and Technology (VIEST).

1. IM Hodge, Physical aging in polymer glasses. *Science* **267**, 1945–1947 (1995).
2. J Zhao, SL Simon, GB McKenna, Using 20-million-year-old amber to test the super-arrhenius behaviour of glass-forming systems. *Nat. Commun.* **4**, 1783 (2013).
3. SF Swallen, et al., Organic glasses with exceptional thermodynamic and kinetic stability. *Science* **315**, 353–356 (2007).
4. K Ishii, H Nakayama, S Hirabayashi, R Moriyama, Anomalously high-density glass of ethylbenzene prepared by vapor deposition at temperatures close to the glass-transition temperature. *Chem. Phys. Lett.* **459**, 109–112 (2008).
5. E Leon-Gutierrez, G Garcia, AF Lopeandia, MT Clavaguera-Mora, J Rodríguez-Viejo, Size effects and extraordinary stability of ultrathin vapor deposited glassy films of toluene. *The J. Phys. Chem. Lett.* **1**, 341–345 (2010).
6. E Leon-Gutierrez, A Sepúlveda, G Garcia, MT Clavaguera-Mora, J Rodríguez-Viejo, Stability of thin film glasses of toluene and ethylbenzene formed by vapor deposition: an in situ nanocalorimetric study. *Phys. Chem. Chem. Phys.* **12**, 14693–14698 (2010).
7. SS Dalal, Z Fakhraai, MD Ediger, High-throughput ellipsometric characterization of vapor-deposited indomethacin glasses. *The J. Phys. Chem. B* **117**, 15415–15425 (2013).
8. KL Kearns, P Krzyskowski, Z Devereaux, Using deposition rate to increase the thermal and kinetic stability of vapor-deposited hole transport layer glasses via a simple sublimation apparatus. *The J. Chem. Phys.* **146**, 203328 (2017).
9. P Luo, et al., Ultrastable metallic glasses formed on cold substrates. *Nat. Commun.* **9**, 1389 (2018).
10. AN Raegen, J Yin, Q Zhou, JA Forrest, Ultrastable monodisperse polymer glass formed by physical vapour deposition. *Nat. Mater.* **19**, 1110–1113 (2020).
11. YZ Chua, M Ahrenberg, M Tylinski, MD Ediger, C Schick, How much time is needed to form a kinetically stable glass? AC calorimetric study of vapor-deposited glasses of ethylcyclohexane. *The J. Chem. Phys.* **142**, 054506 (2015).
12. Y Zhang, Z Fakhraai, Invariant fast diffusion on the surfaces of ultrastable and aged molecular glasses. *Phys. Rev. Lett.* **118**, 066101 (2017).
13. AR Moore, et al., Effects of microstructure formation on the stability of vapor-deposited glasses. *Proc. Natl. Acad. Sci.* **116**, 5937–5942 (2019).
14. JL Thelen, et al., Molecular orientation depth profiles in organic glasses using polarized resonant soft x-ray reflectivity. *Chem. Mater.* **32**, 6295–6309 (2020).
15. KL Kearns, et al., Hiking down the energy landscape: progress toward the kauzmann temperature via vapor deposition. *The J. Phys. Chem. B* **112**, 4934–4942 (2008).
16. MS Beasley, C Bishop, BJ Kasting, MD Ediger, Vapor-deposited ethylbenzene glasses approach "ideal glass" density. *The J. Phys. Chem. Lett.* **10**, 4069–4075 (2019).
17. S Samanta, et al., Exploring the importance of surface diffusion in stability of vapor-deposited organic glasses. *The J. Phys. Chem. B* **123**, 4108–4117 (2019).
18. A Sepúlveda, et al., Accelerated aging in ultrathin films of a molecular glass former. *Phys. Rev. Lett.* **107**, 025901 (2011).
19. Y Zhang, Z Fakhraai, Decoupling of surface diffusion and relaxation dynamics of molecular glasses. *Proc. Natl. Acad. Sci.* **114**, 4915–4919 (2017).
20. Y Zhang, et al., Effect of substrate interactions on the glass transition and length-scale of correlated dynamics in ultra-thin molecular glass films. *The J. Chem. Phys.* **149**, 184902 (2018).
21. J Rafols-Ribe, et al., Kinetic arrest of front transformation to gain access to the bulk glass transition in ultrathin films of vapour-deposited glasses. *Phys. Chem. Chem. Phys.* **20**, 29989–29995 (2018).
22. W Kauzmann, The nature of the glassy state and the behavior of liquids at low temperatures. *Chem. Rev.* **43**, 219–256 (1948).
23. Y Katayama, et al., A first-order liquid–liquid phase transition in phosphorus. *Nature* **403**, 170–173 (2000).
24. A Cadien, et al., First-order liquid-liquid phase transition in cerium. *Phys. Rev. Lett.* **110**, 125503 (2013).
25. PH Poole, F Sciortino, U Essmann, HE Stanley, Phase behaviour of metastable water. *Nature* **360**, 324–328 (1992).
26. S Aasland, PF McMillan, Density-driven liquid–liquid phase separation in the system Al2o3–y2o3. *Nature* **369**, 633–636 (1994).
27. Y Li, J Li, F Wang, Liquid-liquid transition in supercooled water suggested by microsecond simulations. *Proc. Natl. Acad. Sci.* **110**, 12209–12212 (2013).
28. N Giovambattista, T Loerting, BR Lukanov, FW Starr, Interplay of the glass transition and the liquid-liquid phase transition in water. *Sci. Reports* **2**, 390 (2012).
29. A Zhang, Y Jin, T Liu, RB Stephens, Z Fakhraai, Polyamorphism of vapor-deposited amorphous selenium in response to light. *Proc. Natl. Acad. Sci.* **117**, 24076–24081 (2020).
30. MS Beasley, et al., Physical vapor deposition of a polyamorphic system: Triphenyl phosphite. *The J. Chem. Phys.* **153**, 124511 (2020).
31. A Gujral, KA O'Hara, MF Toney, ML Chabinyc, M Ediger, Structural characterization of vapor-deposited glasses of an organic hole transport material with x-ray scattering. *Chem. Mater.* **27**, 3341–3348 (2015).
32. I Lyubimov, et al., Orientational anisotropy in simulated vapor-deposited molecular glasses. *The J. Chem. Phys.* **143**, 094502 (2015).
33. SS Dalal, A Sepúlveda, GK Pribil, Z Fakhraai, MD Ediger, Density and birefringence of a highly stable $\alpha,\alpha,\beta$-trisnaphthylbenzene glass. *The J. Chem. Phys.* **136**, 204501 (2012).
34. DM Walters, R Richert, MD Ediger, Thermal stability of vapor-deposited stable glasses of an organic semiconductor. *The J. Chem. Phys.* **142**, 134504 (2015).
35. T Liu, et al., Birefringent stable glass with predominantly isotropic molecular orientation. *Phys. Rev. Lett.* **119** (2017).
36. SS Dalal, DM Walters, I Lyubimov, JJ de Pablo, MD Ediger, Tunable molecular orientation and elevated thermal stability of vapor-deposited organic semiconductors. *Proc. Natl. Acad. Sci.* **112**, 4227–4232 (2015).
37. K Bagchi, et al., Origin of anisotropic molecular packing in vapor-deposited alq3 glasses. *The journal physical chemistry letters* **10**, 164–170 (2018).
38. KJ Dawson, L Zhu, L Yu, M Ediger, Anisotropic structure and transformation kinetics of vapor-deposited indomethacin glasses. *The J. Phys. Chem. B* **115**, 455–463 (2011).
39. T Liu, et al., The effect of chemical structure on the stability of physical vapor deposited glasses of 1,3,5-triarylbenzene. *The J. Chem. Phys.* **143**, 084506 (2015).
40. NW Ashcroft, ND Mermin, *Solid State Physics.* (Saunders College Publishing), (1976).
41. Z Fakhraai, T Still, G Fytas, MD Ediger, Structural variations of an organic glassformer vapor-deposited onto a temperature gradient stage. *The J. Phys. Chem. Lett.* **2**, 423–427 (2011).
42. X Huang, CB Roth, Changes in the temperature-dependent specific volume of supported polystyrene films with film thickness. *The J. Chem. Phys.* **144**, 234903 (2016).
43. Y Han, X Huang, AC Rohrbach, CB Roth, Comparing refractive index and density changes with decreasing film thickness in thin supported films across different polymers. *The J. Chem. Phys.* **153**, 044902 (2020).
44. K Shankland, AR Kennedy, WIF David, Polymorphism in tetra-aryl biphenyl diamine hole transport materials: resolving the conflicting literature on n, n′-diphenyl-n, n′-bis(3,3′-methylphenyl)-[(1,1′-biphenyl)]-4,4′-diamine by high-resolution powder diffraction. *J. Mater. Chem.* **15**, 4838 (2005).
45. Z Zhang, E Burkholder, J Zubieta, Non-merohedrally twinned crystals ofN,n′-bis(3-methylphenyl)-n,n′-diphenyl-1,1′-biphenyl-4,4′-diamine: an excellent triphenylamine-based hole transporter. *Acta Crystallogr. Sect. C Cryst. Struct. Commun.* **60**, o452–o454 (2004).
46. L Yu, Surface mobility of molecular glasses and its importance in physical stability. *Adv. drug delivery reviews* **100**, 3–9 (2016).

47. C Bishop, A Gujral, MF Toney, L Yu, MD Ediger, Vapor-deposited glass structure determined by deposition rate–substrate temperature superposition principle. *The J. Phys. Chem. Lett.* **10**, 3536–3542 (2019).
48. EC Glor, Z Fakhraai, Facilitation of interfacial dynamics in entangled polymer films. *The J. Chem. Phys.* **141**, 194505 (2014).
49. Y Zhang, et al., Long-range correlated dynamics in ultra-thin molecular glass films. *The J. Chem. Phys.* **145**, 114502 (2016).
50. K Paeng, R Richert, M Ediger, Molecular mobility in supported thin films of polystyrene, poly (methyl methacrylate), and poly (2-vinyl pyridine) probed by dye reorientation. *Soft Matter* **8**, 819–826 (2012).
51. EM Han, LM Do, N Yamamoto, M Fujihira, Crystallization of organic thin films for electroluminescent devices. *Thin Solid Films* **273**, 202–208 (1996).
52. J Tribone, J O'reilly, J Greener, Pressure-jump volume-relaxation studies of polystyrene in the glass transition region. *J. Polym. Sci. Part B: Polym. Phys.* **27**, 837–857 (1989).
53. S Mossa, F Sciortino, Crossover (or kovacs) effect in an aging molecular liquid. *Phys. review letters* **92**, 045504 (2004).
54. L Song, et al., Activation entropy as a key factor controlling the memory effect in glasses. *Phys. Rev. Lett.* **125**, 135501 (2020).
55. L Song, et al., Activation entropy as a key factor controlling the memory effect in glasses. *Phys. Rev. Lett.* **125**, 135501 (2020).
56. Y Jin, Ph.D. thesis (University of Pennsylvania) (2020).